International Journal of Civil Engineering and Technology (IJCIET)
Volume 8, Issue 5, May 2017, pp. 1436–1444, Article ID: IJCIET_08_05_154
Available online at http://www.iaeme.com/IJCIET/issues.asp?JType=IJCIET&VType=8&IType=5
ISSN Print: 0976-6308 and ISSN Online: 0976-6316

EVALUATION OF EQUIVALENT DELAMINATION DRIVING COEFFICIENT IN BONDED CONCRETE OVERLAYS

Olubanwo, A.O., Karadelis, J.N and Abbey, S.J.
School of Energy, Construction and Environment Coventry University, United Kingdom

ABSTRACT

This study investigates failure due to interfacial delamination in a bonded concrete overlay system comprising Polymer Modifies Roller Compacted Concrete (PMRCC) overlay and substrate Ordinary Portland Concrete (OPC). Optimum overlay mix was designed using Composite Desirability Analysis (CDA). Intrinsic complex stresses along the plane of the interface resulting from differential length change and elastic mismatched properties between the two bonded layers were investigated. Distinct delamination cases involving variable structural scales were investigated using both laboratory determined fracture parameters and ANSYS zero-thickness Interface Cohesive Zone Model (ICZM) concept. The FEA results showed that the restraint capacity of the interface varies as a function of overlay structural scale and its associated mismatched elastic parameters.

Key words: Delamination, PMRCC, OPC, FEA, ICZM

Cite this Article: Olubanwo, A.O., Karadelis, J.N and Abbey, S.J.. Evaluation of Equivalent Delamination Driving Coefficient in Bonded Concrete Overlays. *International Journal of Civil Engineering and Technology*, 8(5), 2017, pp. 1436–1444.
http://www.iaeme.com/IJCIET/issues.asp?JType=IJCIET&VType=8&IType=5

1. INTRODUCTION

Deterioration of concrete road pavements, bridge decks and runways caused by cyclic environmental conditions and traffic loads is a problem of significant concern. The use of thin structural bonded concrete overlay is a typical curative measure for strengthening and extending the service life of such structures. However, critical delamination / de-bonding problems at the interface resulting mainly from incompatibility related issues between the overlay and the substrate have been observed during the early-age of curing (Karadelis, et. al, 2012).In terms of thermal and shrinkage induced stresses developing in pavement structural systems, several modelling techniques are available. Numerous techniques ranging from the early closed-form solutions of Westergaard (1926), Bradbury (1938) to approximate two / three-dimensional solutions of Birkeland (1960), Majidzadeh (1988) and Al-Negheimish (1988) have been extensively used. But because the restraint effects of the overlay thickness, interfacial chemical bonding and aggregate interlocking play a major role in evaluating the

ensuing self-equilibrating stresses developing along the plane of the interface under thermal and moisture related movements, recent studies have focused on cracking and de-bonding mechanisms based on differential length change between the substrates and overlay materials. Such studies have unequivocally and progressively been advanced by Silfwerbrand (1997), Bernard (2000), Carlsward (2006) and Kristiawan et. al (2009). Similarly, a previous work by Olubanwo and Karadelis (2015), presented a comprehensive review on the theories and modelling techniques mostly employed for BCO interfacial delamination failure description. While reasonable conclusions were drawn from the review, it was not possible to quantify such conclusions in numerical terms. This will be implemented in this paper employing both experimental and numerical methods. The experimental programme was designed to characterise the test specimens which were subsequently used to calibrate the Finite Element models. The study investigates interfacial delamination failure essentially caused by complex stresses resulting from intrinsic differential length change and mismatched properties between the overlay and the substrate. The description and evaluation of such intrinsic complex stresses relative to overlay thickness is implemented here using zero-thickness Interface Cohesive Zone Model (ICZM) within the concept of non-linear fracture mechanical analysis.

2. EXPERIMENTAL WORK

2.1. Concrete Mix Formulation

The overlay material was designed as a Polymer Modified Roller Compacted Concrete (PMRCC) capable of:(1) resisting roller sinking during vibratory compaction, (2) providing relative compatible movement with the substrate, and (3) exhibiting durable early-age interfacial bond performance. In order to achieve the prescribed multi-criteria requirements of the overlay material, a classical constrained mixture formulation model based on Extreme Vertices Design (EVD) method was adopted. In the model, both lower (L_i) and upper (U_i) bounds were set within $[N(2)^{N-1}+1]$ possible mix space; where, N is the number of components in the mixture. In addition, a composite desirability optimisation function (D) defined by $D = [d(y_1) * d(y_2) * \ldots\ldots\ldots * d(y_n)]^{1/n}$was incorporated such that the optimum mix maximises the weighted geometric mean of individual desirability function ($d(y_i)$) over the entire composite response space. Here, n denotes the total number of all individual responses, while the desirability scale for each prescribed response is constrained within $0 \leq d(y_i) \leq 1$. The conditions for acceptance or rejection therefore depend on the direction of optimisation – i.e. maximum, minimum or target.

2.2. Material Composition, Mixing and Testing

The PMRCC constituents comprised Portland cement CEM I, SBR Polymer Emulsion, Water, Fine aggregate (FA) and Coarse aggregate (CA) and Steel-Fibre (SF). In its fresh state, it has been shown in (Olubanwo and Karadelis, 2014) that resistance to sinking relies on the mix consistency performance, which invariably is contingent on the paste content of the constituents. Following the constraint bounds prescribed in section 2.1 above, a trial paste components proportion shown in Table 2.1 was implemented. This trial mix proportions correspond to variability limits of Water-Cement (W/C) and Polymer-Cement (P/C) ratios ranging between 18% - 22% and 10% - 15% respectively, while the maximum cement content was limited to 635kg. The amounts of CA, FA and SF were held constant at 952.5kg, 635kg and 117kg respectively.

Table 1 Paste Components Proportion (Olubanwo and Karadelis, 2014)

Range Limit	SBR (x_1)	WATER(x_2)	CEMENT (x_3)	TOTAL
Lower	0.078	0.141	0.781	1.0
Upper	0.117	0.172	0.711	1.0

Based on Table 1, an Extreme Vertices Design was implemented with 13 possible mix proportions after constraining the sum of the lower and upper bounds of the possible Paste combination to 1.0. The implementation of the mixture model was done on the initial assumption that a second-degree design will suffice. A total of five runs were carried out for each design point shown in Figure 1(a) per specified response. The Analysis of Variance (ANOVA) and Composite Desirability analysis were subsequently performed with Minitab statistical software (Version, 16) based on the multi-response desirability limits shown in Table 2. In the ANOVA, components and models with p-value ≤ 0.05 were selected as viable.Figure 1 (b)shows the composite desirability response curves based on the input variable settings given in Table 2, and optimisation analysis performed based on the optimisation function (D) given in section 2.1 above. As seen, the composite desirability "D" and the individual desirability depicted by "d" for each predicted property show sufficient closeness to 1. From the results, the predicted optimum response "y" associated with each measured property is also given. The optimum mixture proportion is given by: SBR=0.0938, WATER=0.1523, and CEM 1= 0.7540.

Table 2 Summary of multi-response desirability limit (Olubanwo, 2013)

Measured Property	Set Goal	Lower	Target	Upper	Weight
Consistency-time (sec)	Target	25.0	35.0	40.0	1
Compacted density (%TAFD)	Maximize	96.0	98.0	-	1
Compressive strength (MPa) 3-day	Maximize	31.02	34.4	-	1
Compressive strength (MPa) 28-day	Maximize	48.4	52.2	-	1
Elastic Modulus (GPa) 28-day	Target	21.2	22.3	23.4	1

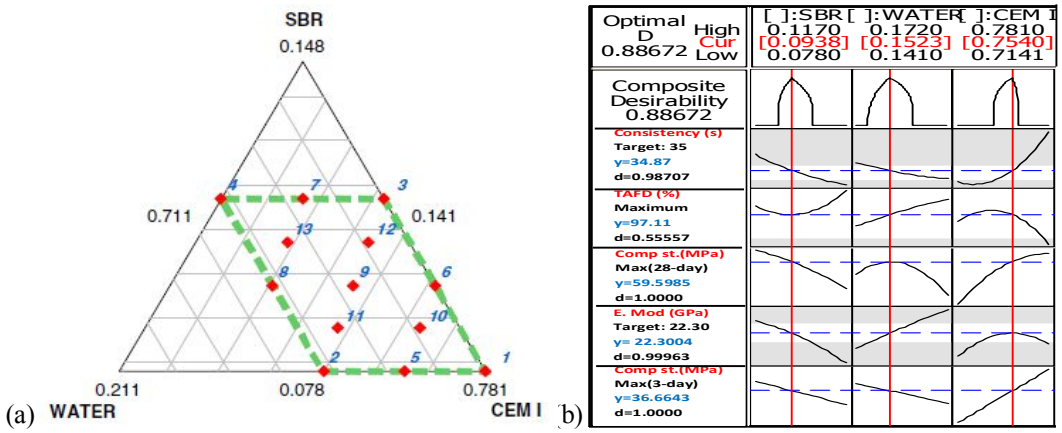

Figure 1 (a) Extreme Vertices Design (b) Composite optimization Response plot

From the optimum mixture proportion deduced from Figure 1(b), Table 3 yields the resulting amount of the overlay PMRCC material by weight. The constituents of the substrate ordinary Portland cement concrete (OPCC) by weight is also appended. Note, the mixing procedure for each batch complied with ASTM C1439-99 (1999), while the test procedures for mix consistency evaluations complied with ASTM C1170 / C1170M-08 (2008) and

ASTM D792 (2008). The compressive and elastic modulus tests were performed in accordance to ASTM 469 (1994) procedures.

Table 3 Optimum PMRCC and OPCC material constituents (Olubanwo, 2013)

Material	CEM I	WATER	SBR	CA	FA	SF	TOTAL
Quantity (kg/m^3)	612.9	123.8	76.2	952.5	635.0	117.0	2517.4
Specific / particle density (kg/m^3)	3150	1000	1040	2770	2670	7800	-
Volume in mixture (m^3)	0.195	0.124	0.073	0.34	0.24	0.015	0.987
OPCC Quantity (kg/m^3)	400	200	-	1116	684	-	2400

Note: Air Content = 100 (1- V_t) = 100 (1-0.987) = 1.3%

Since the overall desirability level shown in Figure 2.1b is considerably satisfactory, the interfacial bond capacity of the optimum mixture with the underlying OPCC substrate was subsequently assessed by employing methods of direct shear-slip and indirect tensile tests shown in Figure 2.

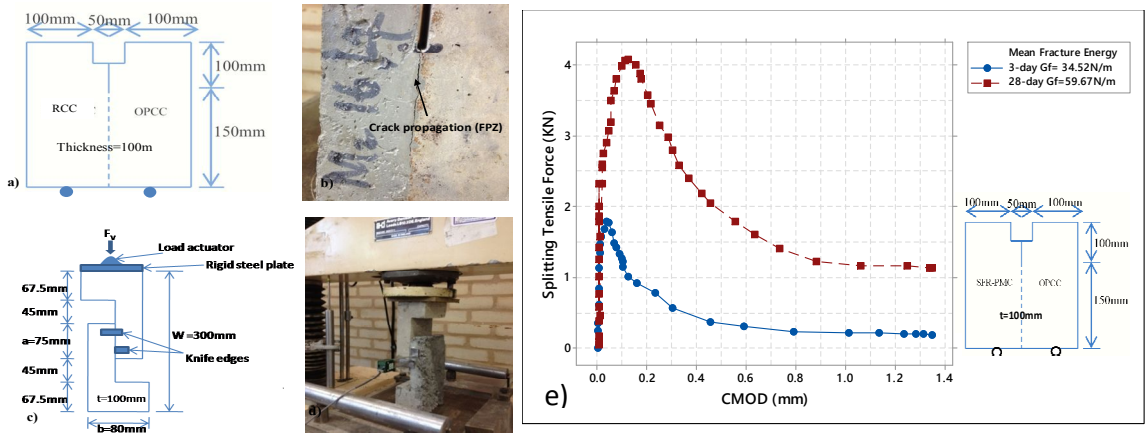

Figure 2 (a & b) Wedge splitting test (c & d) Direct L-Prism shear-slip test (e) Wedge Splitting Force vs. Crack Mouth Opening Displacement

The substrate average roughness value determined by sand-patch measurement method (BS 598-3, 1985; TRRL (1969) for all specimens was approximately 2.3mm. In the wedge splitting test (WST), a loading rate of 0.0016mm/s was used for all test specimens, while the Prismatic Brazilian tensile test loading adhered to BS EN 12390-6:2000 and ASTM C496/ C496Mcontrolled at 0.04 MPa/s. Table 4 shows the resulting interfacial fracture parameters obtained from L-Prism shear-slip and Wedge splitting tests. Note that the cohesive tensile bond strength corresponds to Prismatic Brazilian tensile splitting.

Table 4 Interfacial Fracture parameters for Mode I and Mode II

Failure Mode	Interface Cohesive Failure Criteria			Interface Evolution Contact Parameters	
	Bond Strength(MPa)	Fracture Toughness (N/m)	Critical Opening/slip limit (mm)	Cohesion (MPa) (C)	Friction coefficient (μ)
Mode I	2.07	34.52	0.034	2.14	0.8
Mode II	3.8	179.28	0.108		

Note: $OPCC\rho$=2400kg/m^3; $RCC\rho$=2400kg/m^3; K=2.26W/m.K and α_{coef}= 13.7 x 10^{-6} /K. (where K=thermal conductivity of the overlay, α_{coef}= coefficient of thermal expansion of the overlay)

Table 5 Elastic Mismatched Properties between PMRCC and OPCC

	Measured Elastic Properties				Estimated Mismatched Properties	
Model No	PMRCC Elastic Modulus (GPa)	PMRCC Poisson's ratio (v_1)	OPCC Elastic Modulus (GPa)	OPCC Poisson's ratio (v_2)	Estimated Relative Stiffness (α)	Estimated Relative Compressibility (β)
1	12.9	0.299	22.3	0.2	-0.242	
2	14.3	0.275	22.3	0.2	-0.201	
3	16.8	0.23	22.3	0.2	-0.134	-0.036
4	18.4	0.2	22.3	0.2	-0.096	
5	22.3	0.115	22.3	0.2	-0.014	

Where, $\alpha = \frac{E_1' - E_2'}{E_1' + E_2'}$; $\beta = \frac{E_1'(1-v_1)(1-2v_2) - E_2'(1-v_2)(1-2v_1)}{2(1-v_1)(1-v_2)(E_1' + E_2')}$; $E_i' = E_i/(1-v_i^2)$

3. NUMERICAL MODELLING

Finite Element model idealisation was achieved by assuming that a uniaxial stress condition develops near and parallel to the overlay edges. In this respect, a 2-D plane strain analysis would suffice to analyse the warping/curling effects resulting from either temperature or moisture change through the overlay thickness. In this respect, ensuing stresses are therefore assumed as acting on a beam at the edges rather than on the entire overlay slab. Similar approach has been implemented in Houben (2006) and Olubanwo, et al (2016). In the current study, only negative temperature effect was considered which simulates the intrinsic loading on the overlay due to moisture loss during the early curing age. Hence, in order to simulate such intrinsic strain imposition, an equivalent differential temperature of -14^{0}C derived from the free shrinkage strain provided in Olubanwo (2013) for the same overlay material was applied as a nodal thermal loading on the top surface of the overlay. In order to ensure that all imposed equivalent thermal strains were confined only to the overlay thickness; heat transfer across the interface was precluded via the contact interface element degree(s) of freedom. This is reasonable because not significant further shrinkage is envisaged to occur in an old concrete substrate. The Boundary conditions for the substrate therefore are as shown in Figure 3, while the bonded overlay was allowed to curl freely. The base of the substrate was supported using known prescribed soil properties associated with the surface effect element SURF 153 in ANSYS FEA application.

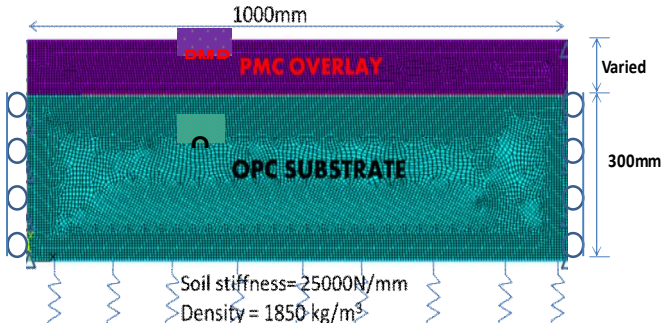

Figure 3 Bonded Concrete Overlay FEM Model

The meshing of the bonded model shown in Figure 3 was accomplished with a 2-D coupled-field plane element (PLANE13) capable of both thermal and structural analysis, while the interface was discretized by a set of target segment (TARGE169) and paired with its associated contact surface element (CONTA171). The elastic foundation employed a surface effect element SURF153 defined by soil stiffness and density. Its stress stiffness matrix and load vector calculations therefore rely on the prescribed in-plane force per unit length and the elastic foundation stiffness. Basically, for delamination to occur along the plane of the interface during the analysis, it's assumed that the de-bonding criteria defined by Table 4 are reached. The model geometry comprises 300mm substrate thickness; 1000mm working pavement length and varied overlay structural thickness of 50, 65, 75, 85 and 100mm. The possible material mismatched elastic properties used for the overlay RCC and the substrate OPCC are given in Table 5.

4. RESULT ANALYSIS AND DISCUSSION

From the 2-D plane strain model described in section 3.0 above, a non-linear contact analysis was performed under an incremental negative thermal loading to evaluate the ensuing mixed-mode fracture energy driving the delamination faliure along the zero-thickness cohesive interface. Here, the delamination driving force is assumed to be controlled or influenced by the local steady-state phase angle ($\Psi = tan^{-1}\left(\frac{\tau}{\langle\sigma\rangle}\right)$) due to the oscillatory field associated with the vicinity of the crack tip. In this respect, the interface attains itscritical fracture condition when the mixed-mode energy release rate G_{ic} equals the fracture toughness of the interface $G_{ic}(\Psi)$. Thus, the normalised interface toughness for the model in section 3.0 is then expressed as a function of the delamination driving coefficient (D_c) denoted by:

$$G_{ic} = D_c(\eta, \alpha, \beta) = \frac{E^* G_{ic}(\Psi)}{\lambda_m^2 h_{overlay}} \qquad (1)$$

Where, $\eta = \frac{h_{overlay}}{h_{total}}$; $E^* = \frac{1}{2}\left(\frac{E_1' . E_2'}{E_1' + E_2'}\right)$; $\lambda_m = \sqrt{\langle\sigma\rangle^2 + \tau^2}$; $h_{overlay}$ is overlay thickness; α and β are Dundur's mismatched elastic parameter defined in Table 5 above. Equation 1 typically corresponds to an extended Hillerborg's characteristic length which permits the delamination driving coefficient (D_c)to be numerically determined as a function of structural scale (η) for different values of $\alpha$for any fixed non-zero value ofβ. Note, the effects of non-zero value of β is generally small and insignificant. Figure 4 a shows a typical curling response of the overlay, while Figures 4.1(b & c) depict the corresponding interface cohesive stress distributions in Mode I and Mode II respectively.

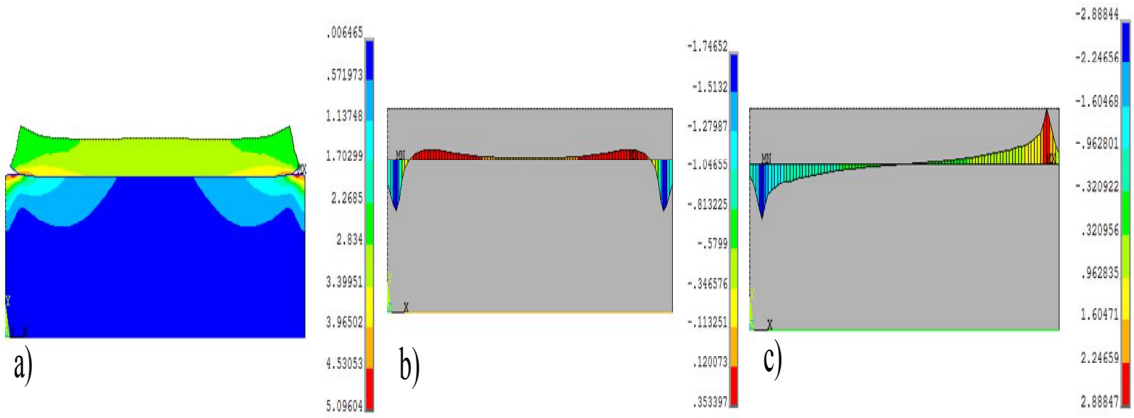

Figure 4 Typical (a) Von Mises Contour Stress (b) Tensile Interfacial cohessive stress (c) Tangential Interfacial cohessive stress

In the results, the interface experiences high debonding stresses at and around its discontinuities, but reduced stresses toward the mid region. In the analysis, the equivalent interfacial mixed-mode fracture enery release was evaluated for each mismatched combination shown in Table 5. Following equation 1, the corresponding delamination coefficient (D_c) denoting the delamination driving energy is illustrated in Figure 4 using a second-degree regression fitting.

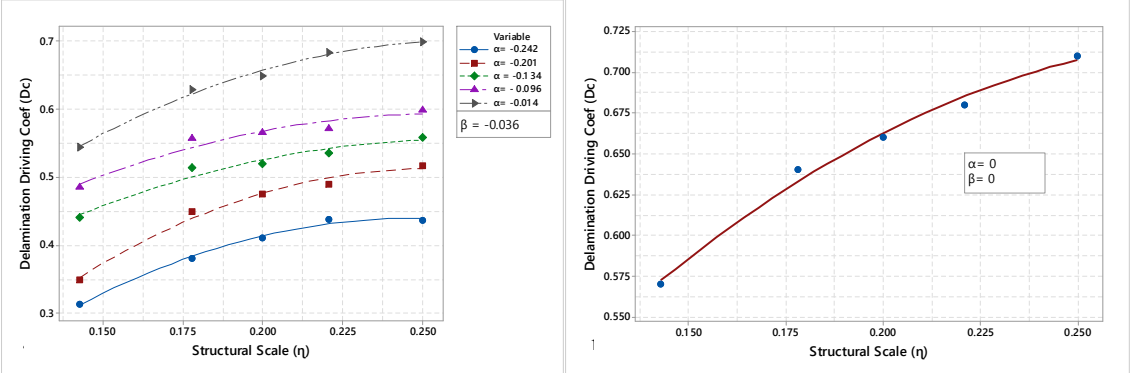

Figure 5 (a & b) Variation of Delamination Driving Coefficient as a function of structural scale for different mismatched elastic properties.

As seen in Figure 5, the interface response curves generally indicate that the driving energy needed to initiate and propagate delamination increases as the normalised structural scale (η) increases. This is because the restraint capacity of the interface increases in value with overlay thickness and self-weight. Similarly, the curves show that since Dundur's first parameter (α) measures the relative stiffness of the bi-material, the delamination driving energy grows incrementally as elastic mismatched parameter approaches zero. In effect, for a perfect elastic matching (where $\alpha = 0$), a significant relative amount of intrinsic force is required to cause and drive de-bonding. Table 6 presents the resulting cohesive lengths (l_{cz}) zone associated with the delamination driving coefficient (D_c) when $\alpha = 0$.

Table 6 Equivalent Delamination Coefficient and Cohesive Zone Length

η	D_c (*when* $\alpha = 0$)	l_{cz}
0.14	0.57	$9/5\pi\ (E^* G_{Fm}/\lambda_m^2)$
0.18	0.64	$2/\pi\ (E^* G_{Fm}/\lambda_m^2)$
0.20	0.66	$29/14\pi\ (E^* G_{Fm}/\lambda_m^2)$
0.22	0.68	$15/7\pi\ (E^* G_{Fm}/\lambda_m^2)$
0.25	0.71	$9/4\pi\ (E^* G_{Fm}/\lambda_m^2)$

5. CONCLUSIONS

From the investigation and results presented above, the following conclusions can be drawn:

- In the results, optimum material mixture for the PMRCC overlay satisfied full consolidation at 34.87 seconds with an acceptable apparent maximum density of 97.11% TAFD.
- The use of computational methods is essential to harmonise the complex interactions between the material mismatched properties and the structural scale effects associated with Bonded Concrete Overlay systems.
- The delamination driving energy or coefficient varies numerically as a function of (1) BCO structural scale, and Dundur's mismatched elastic parameters. Hence, the interface restraint capacities against delamination are increases with overlay thickness and relative stiffness

values. As $\alpha \rightarrow 0$, increased driving energy is needed to initiate or propagate delamination along the plane of the interface.

REFERENCES

[1] Al-Negheimish, A. (1988) 'Bond Strength, Long Term Performance and Temperature Induced Stresses in Polymer Concrete-Portland Cement Concrete Composite Members, PhD. Dissertation, The University of Texas, Austin, Texas.

[2] ASTM C1170 / C1170M - 08 (2008) Standard Test Method for Determining Consistency and Density of Roller-Compacted Concrete Using a Vibrating Table. ASTM International, West Conshohocken, USA.

[3] ASTM D792 (2008) Standard Test Methods for Density and Specific Gravity (Relative Density) of Plastics by Displacement. ASTM International, West Conshohocken, USA.

[4] ASTM C469/C469M (1994) Standard Test Method for Static Modulus of Elasticity and Poisson's Ratio of Concrete in Compression. ASTM International, West Conshohocken, USA.

[5] BS 598-3 (1985) Sampling and examination of bituminous mixtures for roads and other paved areas, Methods for design and physical testing. British Standard Institute

[6] BS EN 12390-6 (2000) "Testing hardened Concrete. Testing Splitting Strength of test specimens," *British Standard Institute.*

[7] Bernard, O. (2000) "Comportement à long termedes elements de structure formés de bétonsd'âges différents". Doctoral thesis, Swiss Federal Institute of Technology No 2283, Lausanne, Switzerland.

[8] Birkeland, H. W. (1960), 'Differential Shrinkage in Composite beams' Journal of the American Concrete Institute, May 1960, pp.1123-1136

[9] Bradbury, R. D., (1938) "Reinforced concrete pavements," *Wire Reinforcement Institute*, Washington DC.

[10] Carlsward, J. (2006). Shrinkage cracking of steel fiber reinforced self compacting concrete overlays: test methods and theoretical modelling. Doctoral Thesis, Lulea University of Technology, Department of Civil and Environmental Engineering, Division of Structural Engineering, Sweden

[11] Houben, L. J. M. (2003) "Structural design of Pavement – Part IV: Design of Concrete Pavements, Lecture Notes CT4860," Faculty of Civil Engineering and Geosciences, TU Delft; Delft.

[12] Karadelis, N.K., Koutselas, K., Lin, Y., Olubanwo, A., and Xu, Y. (2012) Sustainable, Bonded Overlays for the Repair and Strengthening of Concrete Pavements, *Global Magazine of Concrete Society*, 46(07) 34-36. ASTM C1439-99 (1999) Standard test methods for polymer-modified mortar and concrete, ASTM International, West Conshohocken, USA

[13] Kristiawan, S. A., Mahmudah, A. M. H., and Sunarmasto (2009) "Cracking Resistance of Concrete Overlays as Predicted from the Development of Shrinkage Stress. In Procedings of 3rd International Conference on Concrete Repair pp. 157-160. Padua: ICCR

[14] Sankalp Sharan and Dr. D B Raijiwala, Abrasion and Drop Weight Impact Resistance of Coconut Shell Ash Concrete. *International Journal of Civil Engineering and Technology*, 8(2), 2017, pp. 383-389

[15] Majidzadeh, K. (1988) "A Mechanistic Approach to Rigid Pavement Design. In: Stock A.F. ed. *Concrete Pavement*," Elsevier Applied Science Publishers LTD, UK.

[16] Olubanwo A. O. (2013) Optimum design for Sustainable 'Green' Bonded Concrete Overlays: failure due to shear and delamination. PhD Thesis, Department of Civil Engineering, Architecture, and Building, Coventry University

[17] A Review on Fiber Reinforced Concrete, Grija.S, Shanthini.D, Abinaya.S. *International Journal of Civil Engineering and Technology*, 7(6), 2016, pp.386–392.

[18] Olubanwo A. O and Karadelis J. N (2014) "Applied mixture optimization techniques for paste design of bonded roller compacted fibre reinforced polymer modified concrete (BRCFRPMC) overlays", Journal of Materials and Structures, 48(7) 2023-2042.

[19] Olubanwo, A.O.,Karadelis, J.N.,Xu, Y.,Lin, Y.,Phillips, P. (2016). Optimum Design for Sustainable, 'Green' Concrete Overlays. Part III: Interfacial Delamination. Proceedings, *4th International Chinese European Workshop on Functional Pavement Design,* Delft University, The Netherlands, June/July 2016, 1465-1475

[20] Silfwerbrand, J. (1997) 'Stresses and Strains in Composite Concrete Beams subjected to Differential Shrinkage ACI Structural Journal 94(4)

[21] TRRL (1969) "Instructions for Using the Portable Skid Resistance Tester," Road Note 27, *Transport and Road Research Laboratory HMSO.*

[22] G. Lalitha, Dr. C. Sasidhar and Dr. C. Ramachandrudu, A Review Paper on Strength and Durability Studies on Concrete Fine Aggregate Replaced with Recycled Crushed Glass. *International Journal of Civil Engineering and Technology,* 8(2), 2017, pp. 199–202.

[23] Westergaard, H. M. (1926) "Stresses in Concrete Pavements computed by Theoretical Analysis," Public Roads, Vol. 7, No 12, pp.23 – 35.

[24] Olubanwo, A.O. and Karadelis, N.K. (2015) Interfacial Delamination Failure in Bonded Concrete Overlay Systems - A Review of Theories and Modelling Methods. *International Journal of Civil Engineering & Technology (IJCIET)*. 6(5), pp: 85-99.